PCCP

Investigating the Local Structure of Ti Based MXene Materials by Temperature Dependent X-Ray Absorption Spectroscopy

Journal:	*Physical Chemistry Chemical Physics*
Manuscript ID	CP-ART-10-2022-004759.R2
Article Type:	Paper
Date Submitted by the Author:	15-Dec-2022
Complete List of Authors:	Olszewski, Wojciech; University of Bialystok, Faculty of Physics Marini, C.; CELLS, Alba Synchrotron Light Facility Kajiyama, Satoshi; The University of Tokyo, Department of Chemical System Engineering Okubo, Masashi; Waseda University, Department of Electrical Engineering and Bioscience Yamada, Atsuo; The University of Tokyo, Department of Chemical System Engineering, School of Engineering Mizokawa, T.; Waseda University, Department of Applied Physics Saini, Naurang; University of Rome La Sapienza, Department of Physics Simonelli, Laura; CELLS, Alba Synchrotron Light Facility

Investigating the Local Structure of Ti Based MXene Materials by Temperature Dependent X-Ray Absorption Spectroscopy

Wojciech Olszewski,[1] Carlo Marini,[2] Satoshi Kajiyama,[3] Masashi Okubo,[3] Atsuo Yamada,[3]*

Takashi Mizokawa,[4] Naurang Lal Saini,[5] Laura Simonelli[2]*

[1] Faculty of Physics, University of Bialystok, 1L K. Ciolkowskiego Str., 15-245 Bialystok, Poland

[2] ALBA Synchrotron Light Facility, Carrer de la Llum 2-26, 08290 Cerdanyola del Vallés, Barcelona, Spain

[3] Department of Chemical System Engineering, School of Engineering, The University of Tokyo, Tokyo, 113-8656 Japan

[4] Department of Applied Physics, Waseda University, Tokyo 169-8555, Japan

[5] Dipartimento di Fisica, Universitá di Roma “La Sapienza”, 00185 Rome, Italy

ABSTRACT

The local structure of Ti based MXene-type electrode materials have been studied by Ti K-edge X-ray absorption fine structure measurements as a function of temperature to obtain direct information on the local bond lengths and their stiffness. In particular, the parent MAX phases Ti_2AlC and Ti_3AlC_2 and its etched MXene systems are characterized and their properties compared. We find that selective etching has substantial effect on the local structural properties of the Ti based MXene materials. It leads to an increase in the interatomic distances, i.e. decrease in the covalency, and corresponding bond stiffness, that is a likely cause of higher achievable performances. The obtained results underline the importance of the local atomic correlations as limiting factor in the diffusion capacity of ion batteries.

1. INTRODUCTION

Li-ion batteries (LIBs) play a dominant role in today's world of technology, especially for transportation[1] and renewable energy storage.[2,3] However, the development of LIBs has been hindered by safety and cost issues,[4] and the currently used materials operate close to their theoretical limit. For this reason research efforts have been dedicated to developing new electrode materials for LIBs,[5] with higher capacities and lifetimes than the currently used ones.

Materials with large specific surface areas and high-rate performances, such as graphene,[6] titanium oxide (TiO_2) and lithium titanate ($Li_4Ti_5O_{12}$)[4,7,8] are considered as viable electrode candidates due to their unique morphology, which enables fast ion diffusion and offers more ion insertion channels.[9]

Recently, layered MXene type materials[10,11] have given rise to a great deal of interest as electrode materials for lithium-ion secondary batteries.[12–17] This material class consists 2D hexagonal compounds synthesized by the exfoliation of ternary carbides, nitrides, or carbonitrides[18,19] with a formula of $M_{n+1}AX_n$, where M is an early transition metal, A is a III or IV A-group element and X is carbon and/or nitrogen (the so called MAX phase). The exfoliation process is carried out by selectively wet-chemical etching the A layers ending up with 2D layered MXenes with general formula $M_{n+1}X_nT_x$, where T represents surface termination (OH/F groups) and x is the number of the surface groups per formula unit.[10,20,21] Different etching mechanisms or etchants have been proofed to affect structural features and defects, which are of potential critical importance for improving the MXene final properties.[22]

MXenes have been reported with reversible capacities of 110, 170 and 260 mAh/g for Ti_2C-, Nb_2C- and V_2C-based electrodes, respectively, in Li-ion battery cells,[13,15] making some suitable for anodes and others for cathodes. Mentioned values are not as high as 350 mAh/g[23] for the dominant anode material, graphite. The capacity thus needs to be improved. However, in contrary to graphite, MXenes have shown an excellent capability to handle high cycling rates. For example, at a cycling rate of 36C, a reversible capacity of 110 mAh/g was obtained for Ti_3C_2.[12] Additionally, MXene materials are very flexible and durable at the same time - a roller made of $Ti_3C_2T_x$ foil with a thickness of 5 μm is able to support a weight of ~ 4000 times its weight.[21]

Xie et al.[24] reported that Li-ion storage capacities are found to depend on the nature of the surface functional groups in 2d materials. It was shown as well that the local atomic displacements can play key role in diffusion and the reversibility of ions, thus influencing strongly the storage capacities.[25,26] Moreover, the structural features and composition in $Ti_3C_2T_x$ MXene negative electrode has been shown to concur in modulating the electrochemical properties in sodium ion batteries.[27] In particular it has been pointed out how the disorder can be a limiting factor for the ion diffusion, while the nature of the termination is expected to influences more the average electrical potential of the ion intercalation than the specific capacity.[28] Therefore, understanding the influence of the local atomic disorder and bond strength on the performances of the batteries is paramount to achieving optimized and efficient storage devices on the commercial scale.

In the present work we report x-ray absorption fine structure (XAFS) investigation of the Ti based layered MAX phase precursors and MXene electrode materials, where the opened interlayer space between individual 2D $Ti_{n+1}C_nT_x$ (n = 1, 2; T_x = OH/F) units leads to high gravimetric and volumetric capacitances with reduced Li diffusion limitation.[29] The present work is focused on understanding the role of structural disorder and lattice stiffness in defining the general electrode performances.

2. EXPERIMENTAL METHODS

Two series of samples were prepared: Ti_2AlC and Ti_3AlC_2 MAX precursors as well as their Ti_2CT_x and $Ti_3C_2T_x$ MXene phases obtained by HF etching process. Additionally, in case of $Ti_3C_2T_x$ sample second way of etching process was performed – by means of LiF/HCl mixture. All samples were prepared as reported in the literature.[10,11,29–32]

Investigated materials were thoroughly characterized by means of powder X-ray diffraction (XRD), transmission electron microscopy (TEM), energy dispersive X-ray spectroscopy (EDX), and x-ray photoemission spectroscopy (XPS). The detailed information about the samples' characterization, including their electrochemical properties, was reported by Wang et al.[30] and Kajiyama et al.[29,31] The XRD patterns are provided in the Supporting Information.

X-ray absorption measurements at the Ti K-edges were performed in transmission mode at the CLAESS beamline of ALBA Synchrotron Light Facility (Barcelona, Spain).[33] The samples used in presented study were prepared from the same bunch of powders used in characterization process[29–31] and were not more than few months old. Prior the experiment the samples were stored and handled in protective atmosphere of Ar. The samples were finely powdered, well-dispersed in boron nitride (BN) and pressed into 13-mm diameter disks to obtain the Ti K-edge X-ray absorption step close to 1. The storage ring was operating at an energy of 3.0 GeV and an average current of about 150 mA. The radiation was monochromatized by a double-crystal, fixed exit, Si(111) monochromator. Considering the life-time broadening of the Ti K level, the total energy resolution of the spectrum is around 1 eV. The monochromator reproducibility allows for energy shift sensitivity down to 0.05 eV. Higher harmonics were rejected by means of Si and Rh-coated mirrors. Samples were mounted into a liquid nitrogen cryostat and the spectra were recorded in vacuum from 80 to 320 K (within accuracy of 1 K). The intensities of incident and transmitted beams were monitored by ionization chambers, with a combination of He, N_2 and Kr gases for appropriate absorption. Several consecutive scans were acquired at each temperature to ensure the reproducibility of the spectra and to improve the signal to noise ratio. Energy calibration of all spectra was achieved by simultaneous measurements of absorption near Ti K-edge (4966 eV) of 3 μm thick Ti foil.

The quantitative experimental data evaluation was performed using the Athena and Artemis[34] graphical interface of FEFF6 code.[34,35] It was achieved by background subtraction and normalization followed by Fourier filtering and fitting a signal, calculated for a small atomic cluster around the absorber species. The coordination numbers N_i were fixed to the average values known from diffraction studies.[10,36] Prior to refinements, nonstructural parameters (E_0 and S_0^2), that affect EXAFS, were chosen and fixed after a number of fit trials on different scans. The structural parameters of each coordination shell were determined by a non-linear least-square fitting in k space (3–13 Å^{-1}). The number of fitting parameters (R_i, σ_i^2 ~ 8) has been kept below the maximum allowed (N_{ind} = 10 in the present case) which is defined by the Δk = 10 Å^{-1} and ΔR = 1.6 Å ranges used for the fitting: $N_{ind} \sim 2\Delta k \Delta R/\pi$.[37] Further details on the EXAFS data treatment are reported in the Supplementary Information.

To take into account the errors coming from normalization and background subtraction, the uncertainties were estimated by fitting independently the different scans that were merged to achieve the reported statistics.

3. RESULTS AND DISCUSSION

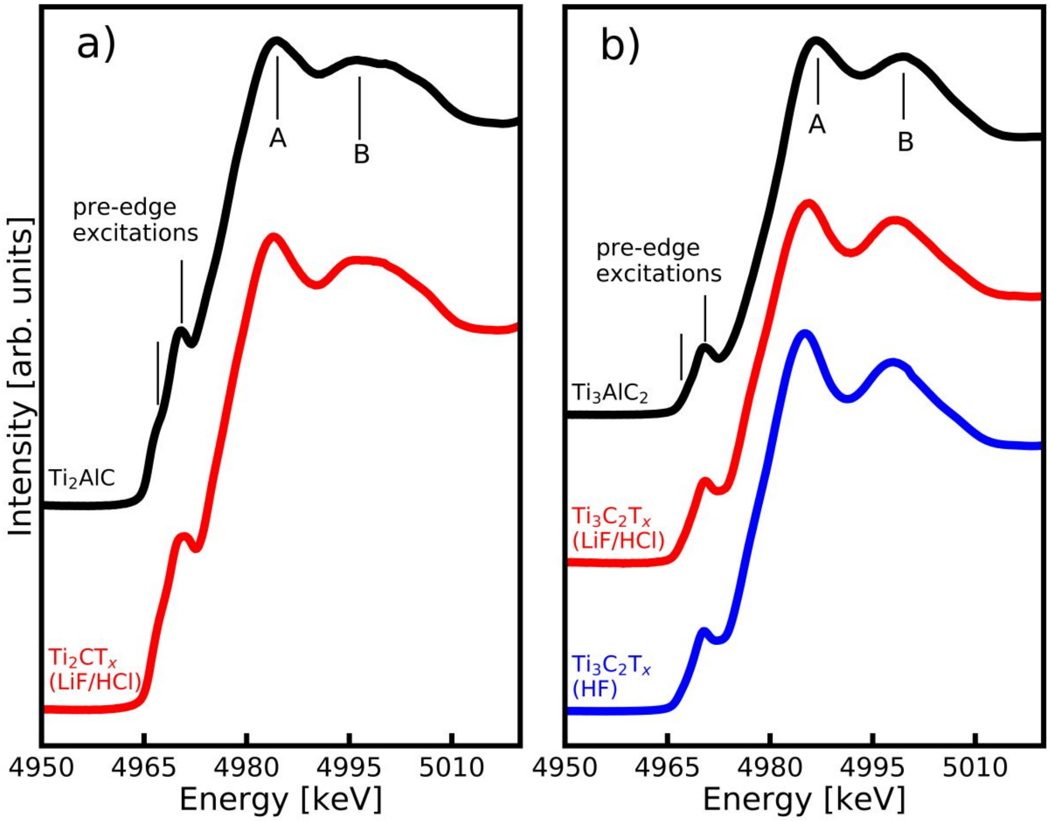

Figure 1. Ti K-edge XANES spectra of a) Ti_2AlC, Ti_2CT_x (LiF/HCl etched) and b) Ti_3AlC_2, $Ti_3C_2T_x$ (LiF/HCl etched), $Ti_3C_2T_x$ (HF etched). All spectra were recorded at 80 K.

Figure 1 shows the Ti K-edge X-ray Absorption Near Edge Structure (XANES) spectra of the investigated materials. Generally, in the investigated temperature range (80-320 K) and in the absence of transitions, the XANES region is not strongly affected by temperature. Since this is the case, only the spectra measured at 80 K are presented. The pre-edge absorption peak around 4970 eV corresponds primarily to the transition from Ti $1s$ to Ti $3d$ hybridized with C $2p$ orbitals[38–40] and other dipolar excitations, where the overall intensity of the quadrupolar peak components depends on the $3d$-$2p$ hybridization. In the case of $Ti_3C_2T_x$ the pre-edge region is almost unaffected during the etching process, while for Ti_2CT_x the split between the low energy peaks positions have decreased by ~0.15 eV with respect to the Ti_2AlC, indicating a possible electronic bands reorganization.[41,42] In addition, the $Ti_3C_2T_x$ spectrum shows lower pre-peak intensity in compare to that for Ti_2CT_x, indicating reduced hybridization in the earlier.[41]

The main-edge region shows two peaks (denoted as A and B on Figure 1) originate from Ti $1s$ to $4p$ excitations.[41] The positions of those peaks are almost the same in pristine and etched samples, which suggests that the interaction between the Al and the Ti_2C or Ti_3C_2 layers are very weak. Small shift (~0.4 and 0.6 eV for Ti_2CT_x and $Ti_3C_2T_x$, respectively) is most probably the consequence of the replacement of the Al layers during the etching process with the termination species T_x strongly attracting charge from the Ti atoms.[27] In addition, in the case of Ti_2AlC and Ti_2CT_x samples, peak B reveals a shoulder at 5003.5 eV. This feature shows some similarities to the XANES spectrum of TiO_2,[43] that suggests a stronger Ti-T_x interaction in Ti_2CT_x compared to the $Ti_3C_2T_x$.

Although the XANES did not show significant differences in spectral shape, edge shifts can be clearly recognized. The edge energies of Ti_2CT_x (4966.9 eV) and $Ti_3C_2T_x$ (4967.2 eV) are close to that of TiC (4967.1 eV), which is between the energies of Ti foil (4966.4 eV) and TiO_2 (4968.6 eV), indicating its carbide nature.[27,41,44,45] The reported energy shifts are consistent with a decrease in the average oxidation state of the Ti atoms in the Ti_2CT_x system respect the $Ti_3C_2T_x$ counterpart.[44] However, the shapes of the XANES spectral profiles of Ti_2CT_x and Ti_3C_2Tx in respect to Ti_2AlC and Ti_3AlC_2, respectively are still quite similar, indicating that the average geometry of the material was well preserved after the removal of Al layers.

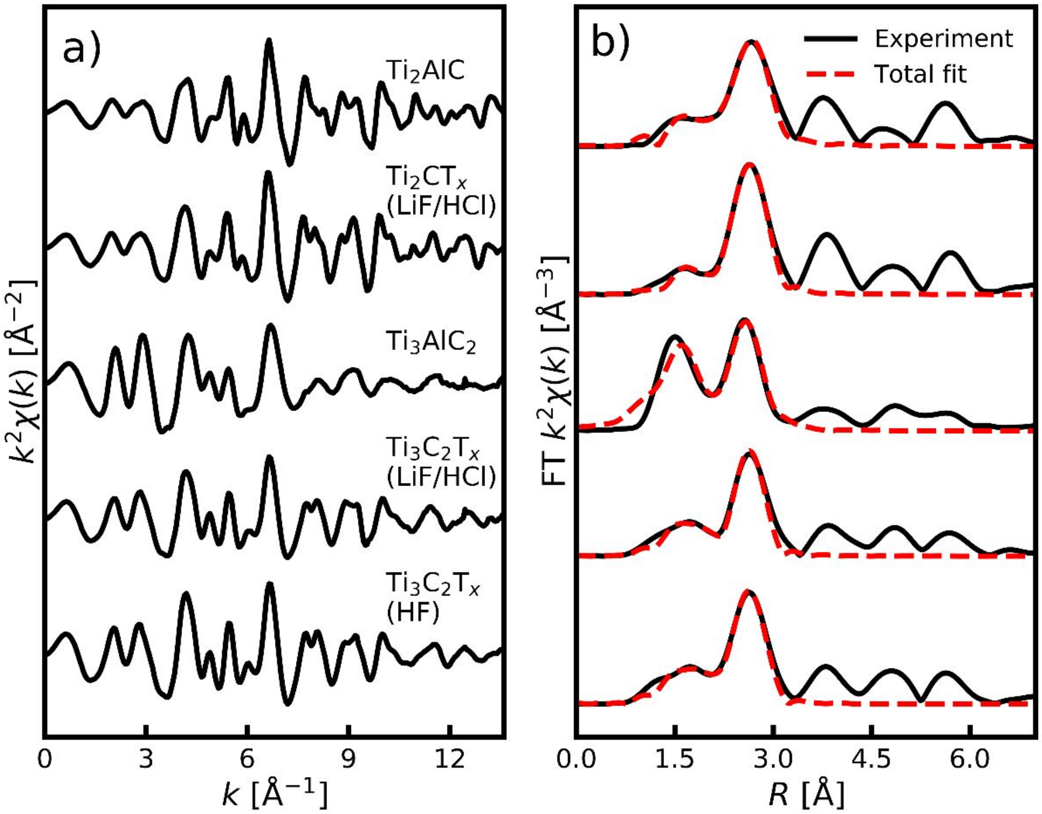

Figure 2. a) k^2-weighted EXAFS signals of the Ti_2AlC, Ti_2CT_x (LiF/HCl etched), Ti_3AlC_2, $Ti_3C_2T_x$ (LiF/HCl etched), $Ti_3C_2T_x$ (HF etched) recorded at 80 K and b) the corresponding to those signals Fourier transforms with the best theoretical description.

Figure 2a and 2b show the evolution of the k^2-weighted Extended X-ray Absorption Fine Structure (EXAFS) oscillations and their relative Fourier Transforms (FT) relative to the spectra collected at 80 K. The amplitude of the EXAFS oscillations and the peak intensity in the FT increases as the measurement temperature decreases (not shown here), due to a progressive freezing of the thermal fluctuations. The low temperature spectra allow a higher resolution to address details in the local structure and have been chosen as representative. The FTs for all show two broad single scattering contributions at around 1.5 and 2.6 Å. The first peak corresponds to the superimposed Ti-C and Ti-Al (only for MAX phases) scattering, whereas the second peak corresponds to the in- and out-of-plane Ti-Ti scattering. The Ti_3AlC_2 MAX phase shows a particular intense FT first contribution, differently to what was reported for the same system in the literature.[42] It suggests a possible dependence of the synthesis roots on the final local structure. Such strong feature could be also associated to a partial degradation of the sample in humid atmosphere.[46–48] Since the strong hydrophilic properties of the MXenes[21] the presence of the water could preferably lead to its reaction with the most active flake edges, ending with Ti oxidation,[49] unlikely in the present case since no air/water exposure. The corresponding MXene compound is instead showing a weak FT first contribution, similar to what reported into the literature,[42,49] and comparable to the Ti_2AlC and Ti_2CT_x systems. The second FT feature, at 2.6 Å, is of comparable intensity for all the investigated samples. The peaks appearing at longer distances ($R > 3$ Å) are due to single scattering contributions of distant shells and multiple scattering involving different paths. For the quantification of the local structure, the EXAFS oscillations were modeled using the general standard equation, assuming the single-scattering approximation:

$$\chi(k) = \sum_{i} \frac{N_i S_o^2}{kR_i^2} f_i(k, R_i) e^{\frac{-2R_i}{\lambda}} e^{-2k^2\sigma_i^2} \sin\left[2kR_i + \delta_i(k)\right] \tag{1}$$

where N_i is the number of neighboring atoms at a distance R_i from the absorbing atom, S_0^2 is the passive electron reduction factor, $f_i(k, R_i)$ is the backscattering amplitude, λ is the photoelectron mean free path, $\delta_i(k)$ is the phase shift, and σ_i^2 is the Debye-Waller factor measuring the mean square relative displacements (MSRDs) of the photo-absorber backscatter pairs.

The EXAFS signal was fitted starting from the Ti_2AlC and Ti_3AlC_2 MAX phase structures having the $P6_3/mmc$ space group[27] and composed of alternative stacking of edge-shared Ti_6C octahedra and two-dimensional close-packed Al plane.[50] Whereas the structures of their MXene counterparts were composed of Ti and C atomic layers arranging alternately forming edge-shared Ti_6C octahedra with OH/F terminations (indistinguishable by means of EXAFS) on nonspecial positions.[51]

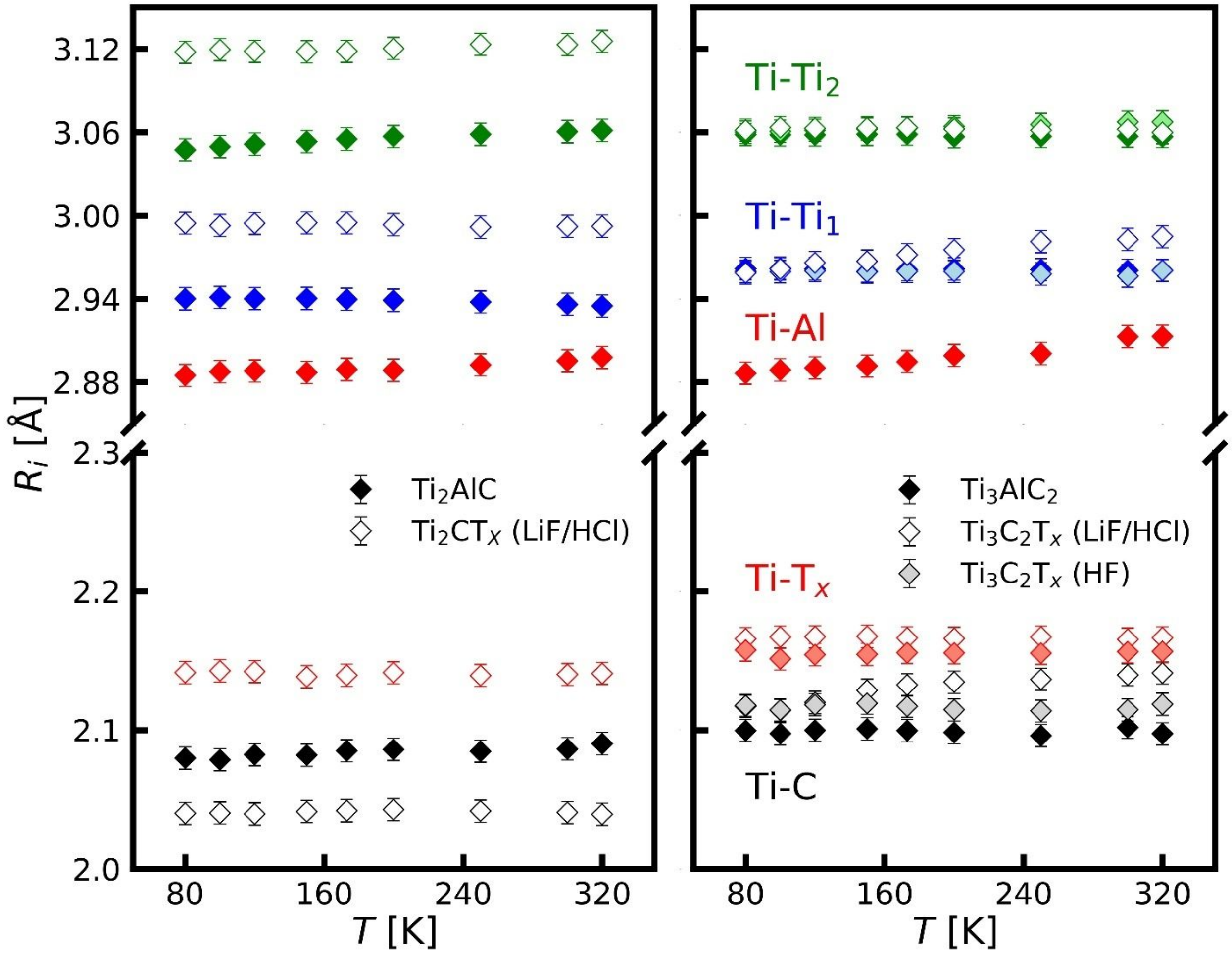

Figure 3. Evolution of the Ti-X bond lengths (X = C, Al/T_x, Ti_1 and Ti_2) in investigated samples (obtained by the EXAFS analysis) shown as a function of temperature. The error bars represent standard deviation, determined by analyzing three different EXAFS scans.

Figure 3 shows the temperature dependence of the interatomic distances in all investigated samples obtained by the EXAFS analysis (where Ti_1 and Ti_2 notation refers to first and second Ti neighboring atom). The measured distances at room temperature are consistent with those known from the crystallographic studies.[10,36,52] As expected, all the investigated interatomic distances tend to decrease with the decreasing temperature. However, differences can be identified in between the bonds and the samples. Indeed, The Ti-C thermal contraction is more pronounced for the Ti_2AlC respect the Ti_3AlC_2 system, while it clearly reverses by etching with LiF/HCl mixture. Moreover, the LiF/HCl etching affect differently the Ti-C bonds on the two systems, with Ti_2CT_x showing a more contracted Ti-C bond.

In general, the selective etching (Al layer removal) influences all the bond lengths, with a minor effect for the Ti_3AlC_2 system. The bond lengths tend to expand by etching, except the Ti-C bond in Ti_2CT_x, which shows a significant contraction, probably to compensate the Ti-Ti elongation. Instead, in the case of the Ti_3AlC_2 system, the Ti-Ti bonds shows a small expansion, while the Ti-C bond elongates significantly by etching. In this case, the etching with LiF/HCl affects the bond lengths more significantly than with that of HF. Differently from the other shells, the Ti-T_x bond distance is not affected by temperature. In the case of LiF/HCl etching it looks expanded for the $Ti_3C_2T_x$ respect the T_2CT_x sample. Moreover, HF etching slightly contracts the Ti-T_x bond on $Ti_3C_2T_x$ system.

On an average, the thermal contraction is more pronounced for Ti_2AlC in comparison to that for Ti_3AlC_2. Interestingly it is the opposite once the latter is etched by LiF/HCl, mainly for the Ti-C and Ti-Ti_2 bonds. The Ti-Ti_1 contraction is negligible on both parent systems, while it increases only for Ti_3AlC_2 after the chemical etching.

A local bond shortening can indicate an increase in the bond covalency and probably a reduced reactivity.[53,54] The results suggest a stronger covalent nature of the Ti-C and Ti-Ti bonds in Ti_3AlC_2 than that in Ti_2AlC, and inverted tendency by chemical etching. Indeed, the chemical etching seems to strongly distort the local structure of Ti_2AlC, probably reducing the conductive carbide layer flexibility. Instead, the chemical etching on Ti_3AlC_2 induces smaller changes, most likely permitting a more flexible lattice. By comparing the LiF/HCl and HF etching effects on the Ti-C bond distance, the latter seems the most promising, since it reduces the Ti-C covalency, thus favoring its reactivity, and the local thermal expansion, probably because smaller interatomic distribution, which could favor the ion diffusion.[55]

Temperature dependence of the EXAFS signal was used to quantify the local lattice rigidity and the local structural disorder, parameters potentially affecting the ion diffusion. The obtained σ_i^2 of the Ti–C, Ti-Al, $Ti-Ti_1$ and $Ti-Ti_2$ pairs as a function of temperature for different samples are shown in Figure 4.

The σ_i^2 is a sum of temperature independent term (σ_0^2), which describes the static configurational disorder, and a temperature-dependent term (σ^2), i.e., $\sigma_i^2(T) = \sigma_0^2 + \sigma^2(T)$.[56] The measured temperature dependence can be expressed by the Einstein model:[57,58]

$$\sigma^2(T) = \sigma_0^2 + \frac{\hbar^2}{2k_B\mu\theta_E}\coth\left(\frac{\theta_E}{2T}\right) \quad (2)$$

where μ is the reduced mass of the atom pairs, k_B is the Boltzmann constant, and θ_E is the Einstein temperature. The θ_E of different bond lengths can be obtained by the Einstein model fits, thus finding the Einstein frequency, $\omega_E = k_B\theta_E/\hbar$, which is related to the effective bond stretching force constant, $\kappa = \mu\omega_E^2$. Figure 4 shows the $\sigma_i^2(T)$ of the bond lengths in all of the investigated materials together with the corresponding Einstein model fits. All the obtained local structure parameters are summarized in Table 1.

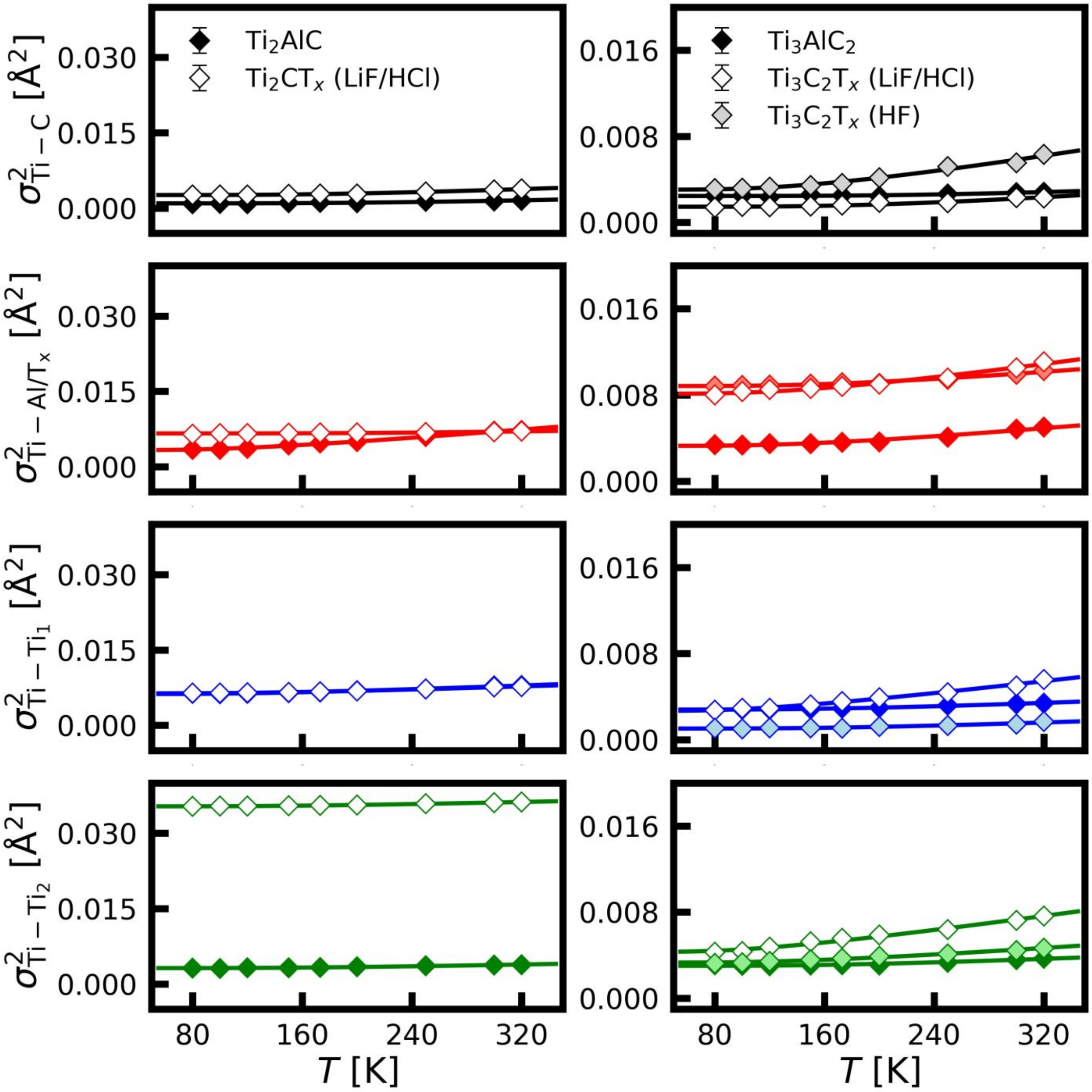

Figure 4. Temperature dependence of the mean-square relative displacements (σ^2) for Ti−X bond lengths (X = C, Al/T_x, Ti_1 and Ti_2). The solid lines are the Einstein model fits. The maximum uncertainty is within the size of graphical representation of the point.

Table 1. Local structure parameters of investigated MXene materials determined by Ti K-edge EXAFS analysis: Einstein temperatures (θ_E), effective bond stretching force constants (κ), temperature independent MSRDs (σ_0^2) and a misfit between data and theory factor, averaged over all temperatures (R).

		Ti_2AlC	Ti_2CT_x (LiF/HCl)	Ti_3AlC_2	$Ti_3C_2T_x$ (LiF/HCl)	$Ti_3C_2T_x$ (HF)
θ_E [K]	Ti-C	784(20)	649(22)	899(27)	706(19)	474(26)
	Ti-Al	349(25)	-	485(20)	-	-
	$Ti-T_x$	-	819(20)	-	459(23)	586(16)
	$Ti-Ti_1$	429(14)	459(27)	597(23)	358(23)	616(30)
	$Ti-Ti_2$	572(10)	538(17)	589(25)	333(27)	462(16)
κ [eV·Å^{-2}]	Ti-C	10.50(54)	7.18(49)	13.80(83)	8.50(46)	3.83(42)
	Ti-Al	3.73(54)	-	7.21(60)	-	-
	$Ti-T_x$	-	14.29(65)	-	4.49(72)	7.32(54)
	$Ti-Ti_1$	7.82(51)	8.96(98)	15.15(92)	5.45(70)	16.13(91)
	$Ti-Ti_2$	13.91(47)	12.31(78)	14.75(95)	4.72(77)	9.08(63)
σ_0^2 [10^{-3} Å^2]	Ti-C	0.95(13)	2.61(14)	2.46(12)	1.46(11)	3.05(13)
	Ti-Al	3.32(14)	-	3.27(12)	-	-
	$Ti-T_x$	-	6.62(15)	-	8.11(18)	8.83(21)
	$Ti-Ti_1$	6.24(13)	6.36(15)	2.79(14)	2.68(12)	1.03(16)
	$Ti-Ti_2$	3.14(16)	35.34(20)	3.01(16)	4.31(15)	3.31(16)
R		0.023	0.022	0.027	0.026	0.023

While the static disorder, represented by σ_0^2, is comparable on the different bonds for the Ti_3AlC_2 sample, it is particularly small (high) for the Ti-C ($Ti-Ti_1$) bond in Ti_2AlC. LiF/HCl chemical etching of Ti_2AlC strongly increases the static disorder relative for the Ti-C and Ti-Ti_2 bonds, leaving the Ti-Ti_1 unaffected. In the case of Ti_3AlC_2 the static disorder is less affected by chemical etching. The Ti-Ti_1 shell has smaller disorder than the Ti-Ti_2 by etching with, in general, a stronger effect for the HF etching. Instead, the Ti-C bond in $Ti_3C_2T_x$ gets more ordered and disordered for LiF/HCl and HF etching, respectively. The Ti-T_x disorder results lower for the Ti_2CT_x than the $Ti_3C_2T_x$ system, with higher disorder corresponding to longer Ti-T_x bond and lower specific capacitance[29] (see Figure 5).

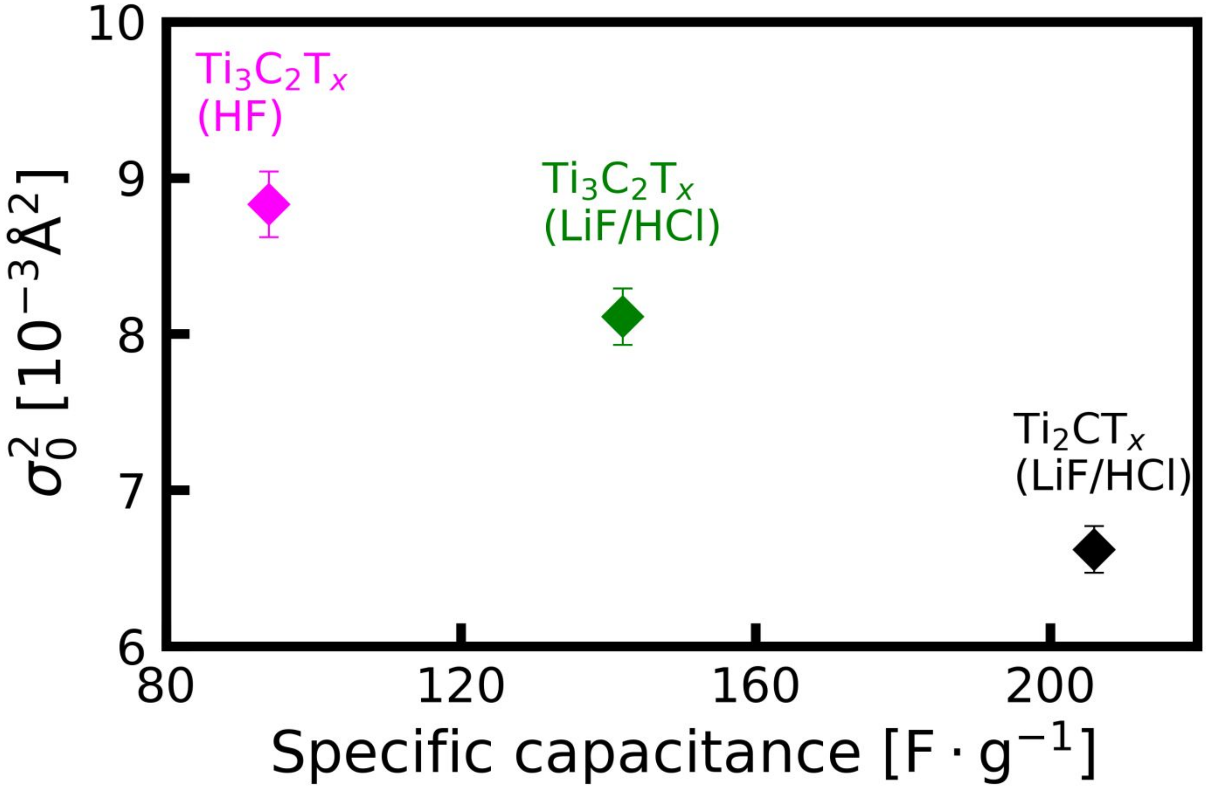

Figure 5. The dependence between Ti-T_x static disorder (σ_0^2) and specific capacitance[29] for investigated MXene materials.

The Einstein temperatures derived from the fits were used to obtain the effective bond-stretching force constant κ, i.e., the bond stiffness. In general, the local bonds in Ti_2AlC are softer than those in Ti_3AlC_2. The results show an overall tendency of bond softening after the etching process. In Ti_2CT_x only the Ti-C bond gets significantly softer by LiF/HCl etching. Instead, in $Ti_3C_2T_x$ all the bonds are getting significantly softer. Such effect is stronger (weaker) for the Ti-C (Ti-Ti) bonds for the HF etching. Instead, for the LiF/HCl etching it is the contrary, the softening is relatively stronger on the Ti-Ti shell in compare to that for Ti-C one. The Ti-T_x bond appear to be harder for the Ti_2CT_x respect the $Ti_3C_2T_x$ system, and for LiF/HCl etching.

The detected bond softening can lead to the increased battery capacity, since more flexible lattice helps in ions diffusion and storage in 2D layered structures.[25,59] Also, a reduced structural disorder is expected to favor the ions diffusion.[60–63] Moreover, a softer lattice is expected to favor reactivity,[64] thus limiting the battery life in case of the studied materials are used as electrodes. After the HF etching of Ti_3AlC_2, the Ti_3C_2 layers are modified with a strong impact on the Ti-C bonds, while, after the LiF/HCl etching, the impact is on the Ti-Ti bonds rather than the Ti-C bonds strength. This indicates that the local lattice properties can be controlled by the modification of the Ti_3C_2 layers by different selective etchings. More recently, selective modifications of the Ti_3C_2 layers have been realized by means of molten salt synthesis.[65,66] In future, the local lattice properties can be controlled by the selective modifications of the $M_{n+1}X_n$ layers in a more systematic manner in order to explore emerging physical and chemical properties of MXenes.

4. CONCLUSIONS

In summary, by means of Ti K-edge x-ray absorption spectroscopy the MAX phase materials Ti_3AlC_2 and Ti_2AlC, and the corresponding MXene materials $Ti_3C_2T_x$ and Ti_2CT_x have been investigated. While the XANES region provides information about the Ti local electronic properties evolution as a function of selective etching (HF and LiF/HCl), temperature dependent EXAFS data allow to access the static disorder and bond characteristics of the investigated materials. The etching procedure leads to increase of the interatomic distances and softening of the bond strengths. While the HF (LiF/HCl) etching of Ti_3AlC_2 (Ti_2AlC), mainly impact on the Ti-C bonds, the LiF/HCl etching of Ti_3AlC_2 mainly affect the Ti-Ti bonds strength, where bond softening can lead to the increased battery capacity. Since the opened interlayer space induced by etching leads to high gravimetric and volumetric capacitances with reduced Li diffusion limitation and with different electrochemical properties depending by the termination species, the obtained results underline the importance of the local atomic correlations as limiting factors in the ion diffusion and capacity of MXene based batteries.

AUTHOR CONTRIBUTIONS

Wojciech Olszewski: investigation, formal analysis, visualization, and writing – original draft & editing; Carlo Marini: investigation; Satoshi Kajiyama: sample preparation, and characterization; Masashi Okubo: sample preparation, and characterization; Atsuo Yamada: sample preparation; Takashi Mizokawa: conceptualization, and review; Naurang Lal Saini: conceptualization, and writing – review; Laura Simonelli: conceptualization, investigation, supervision, and writing – review and editing.

CONFLICTS OF INTEREST:

There are no conflicts to declare.

ACKNOWLEDGMENTS

The authors thank the ALBA CLAESS beamline staff for the support during the experiment. M.O. and A.Y. were financially supported by JST, CREST Grant Number JPMJCR21O6, Japan. M.O. was financially supported by JPSP KAKENHI (Grant Number JP21H04697). T.M. was supported by JSPS KAKENHI (Grant Number JP19H01853). This work was partly supported by joint research program of ZAIKEN, Waseda University (Project No.31010).

REFERENCES

1 F. T. Wagner, B. Lakshmanan and M. F. Mathias, Electrochemistry and the future of the automobile, *J. Phys. Chem. Lett.*, 2010, **1**, 2204–2219.

2 J.-M. Armand, M.; Tarascon, Building better batteries, *Nature*, 2008, **451**, 652–657.

3 B. Kang and G. Ceder, Battery materials for ultrafast charging and discharging, *Nature*, 2009, **458**, 190–193.

4 J. B. Goodenough and Y. Kim, Challenges for rechargeable Li batteries, *Chem. Mater.*, 2010, **22**, 587–603.

5 P. Poizot, S. Laruelle, S. Grugeon, L. Dupont and J. Tarascon, Nano-sized transition-metaloxidesas, *Nature*.

6 E. J. Yoo, J. Kim, E. Hosono, H. S. Zhou, T. Kudo and I. Honma, Large reversible Li storage of graphene nanosheet families for use in rechargeable lithium ion batteries, *Nano Lett.*, 2008, **8**, 2277–2282.

7 P. Reale, S. Panero, B. Scrosati, J. Garche, M. Wohlfahrt-Mehrens and M. Wachtler, A Safe, Low-Cost, and Sustainable Lithium-Ion Polymer Battery, *J. Electrochem. Soc.*, 2004, **151**, A2138.

8 Z. Yang, D. Choi, S. Kerisit, K. M. Rosso, D. Wang, J. Zhang, G. Graff and J. Liu, Nanostructures and lithium electrochemical reactivity of lithium titanites and titanium oxides: A review, *J. Power Sources*, 2009, **192**, 588–598.

9 J. Liu and X. W. Liu, Two-dimensional nanoarchitectures for lithium storage, *Adv. Mater.*, 2012, **24**, 4097–4111.

10 M. Naguib, M. Kurtoglu, V. Presser, J. Lu, J. Niu, M. Heon, L. Hultman, Y. Gogotsi and

M. W. Barsoum, Two-dimensional nanocrystals produced by exfoliation of Ti 3AlC 2, *Adv. Mater.*, 2011, **23**, 4248–4253.

11 M. Ghidiu, M. R. Lukatskaya, M. Q. Zhao, Y. Gogotsi and M. W. Barsoum, Conductive two-dimensional titanium carbide 'clay' with high volumetric capacitance, *Nature*, 2015, **516**, 78–81.

12 O. Mashtalir, M. Naguib, V. N. Mochalin, Y. Dall'Agnese, M. Heon, M. W. Barsoum and Y. Gogotsi, Intercalation and delamination of layered carbides and carbonitrides, *Nat. Commun.*, 2013, **4**, 1–7.

13 M. Naguib, J. Halim, J. Lu, K. M. Cook, L. Hultman, Y. Gogotsi and M. W. Barsoum, New two-dimensional niobium and vanadium carbides as promising materials for li-ion batteries, *J. Am. Chem. Soc.*, 2013, **135**, 15966–15969.

14 J. Come, M. Naguib, P. Rozier, M. W. Barsoum, Y. Gogotsi, P.-L. Taberna, M. Morcrette and P. Simon, A Non-Aqueous Asymmetric Cell with a Ti2C-Based Two-Dimensional Negative Electrode, *J. Electrochem. Soc.*, 2012, **159**, A1368–A1373.

15 M. Naguib, J. Come, B. Dyatkin, V. Presser, P. L. Taberna, P. Simon, M. W. Barsoum and Y. Gogotsi, MXene: A promising transition metal carbide anode for lithium-ion batteries,

Electrochem. commun., 2012, **16**, 61–64.

16 H. Aghamohammadi, R. Eslami-Farsani and E. Castillo-Martinez, Recent trends in the development of MXenes and MXene-based composites as anode materials for Li-ion batteries, *J. Energy Storage*, 2022, **47**, 103572.

17 N. Thakur, P. Kumar, D. C. Sati, R. Neffati and P. Sharma, Recent advances in two-dimensional MXenes for power and smart energy systems, *J. Energy Storage*, 2022, **50**, 104604.

18 M. W. Barsoum, in *Encyclopedia of Materials Science and Technology*, Elsevier, Amsterdam, 2006.

19 M. W. Barsoum, *MAX Phases: Properties of Machinable Ternary Carbides and Nitrides*, Wiley, Hoboken, 2013.

20 S. J. Kim, M. Naguib, M. Zhao, C. Zhang, H. T. Jung, M. W. Barsoum and Y. Gogotsi, High mass loading, binder-free MXene anodes for high areal capacity Li-ion batteries, *Electrochim. Acta*, 2015, **163**, 246–251.

21 Y. Anasori, B.; Lukatskaya, M. R.; Gogotsi, 2D metal carbides and nitrides (MXenes) for energy storage, *Nat. Rev. Mater.*, 2017, **2**, 16098.

22 Y. J. Kim, S. J. Kim, D. Seo, Y. Chae, M. Anayee, Y. Lee, Y. Gogotsi, C. W. Ahn and H. T. Jung, Etching Mechanism of Monoatomic Aluminum Layers during MXene Synthesis, *Chem. Mater.*, 2021, **33**, 6346–6355.

23 M. Tarascon, J.-M.; Armand, Issues and challenges facing rechargeable lithium batteries, *Nature*, 2001, **414**, 359–367.

24 Y. Xie, M. Naguib, V. N. Mochalin, M. W. Barsoum, Y. Gogotsi, X. Yu, K. W. Nam, X. Q. Yang, A. I. Kolesnikov and P. R. C. Kent, Role of surface structure on li-ion energy storage capacity of two-dimensional transition-metal carbides, *J. Am. Chem. Soc.*, 2014, **136**, 6385–6394.

25 W. Olszewski, M. Ávila Pérez, C. Marini, E. Paris, X. Wang, T. Iwao, M. Okubo, A. Yamada, T. Mizokawa, N. L. Saini and L. Simonelli, Temperature Dependent Local Structure of NaxCoO2 Cathode Material for Rechargeable Sodium-Ion Batteries, *J. Phys. Chem. C*, 2016, **120**, 4227–4232.

26 W. Olszewski, I. Isturiz, C. Marini, M. Avila, M. Okubo, H. Li, H. Zhou, T. Mizokawa, N. L. Saini and L. Simonelli, Effects of nanostructuring on the bond strength and disorder in V2O5 cathode material for rechargeable ion-batteries, *Phys. Chem. Chem. Phys.*, 2018, **20**,

15288–15292.

27 C. Ferrara, A. Gentile, S. Marchionna, I. Quinzeni, M. Fracchia, P. Ghigna, S. Pollastri, C. Ritter, G. M. Vanacore and R. Ruffo, The Missing Piece: The Structure of the Ti3C2TxMXene and Its Behavior as Negative Electrode in Sodium Ion Batteries, *Nano Lett.*, 2021, **21**, 8290–8297.

28 A. Gentile, C. Ferrara, S. Tosoni, M. Balordi, S. Marchionna, F. Cernuschi, M. H. Kim, H. W. Lee and R. Ruffo, Enhanced Functional Properties of Ti3C2Tx MXenes as Negative Electrodes in Sodium-Ion Batteries by Chemical Tuning, *Small Methods*, 2020, **4**, 2000314.

29 S. Kajiyama, L. Szabova, H. Iinuma, A. Sugahara, K. Gotoh, K. Sodeyama, Y. Tateyama, M. Okubo and A. Yamada, Enhanced Li-Ion Accessibility in MXene Titanium Carbide by Steric Chloride Termination, *Adv. Energy Mater.*, 2017, **7**, 1–8.

30 X. Wang, S. Kajiyama, H. Iinuma, E. Hosono, S. Oro, I. Moriguchi, M. Okubo and A. Yamada, Pseudocapacitance of MXene nanosheets for high-power sodium-ion hybrid capacitors, *Nat. Commun.*, 2015, **6**, 1–6.

31 S. Kajiyama, L. Szabova, K. Sodeyama, H. Iinuma, R. Morita, K. Gotoh, Y. Tateyama, M. Okubo and A. Yamada, Sodium-Ion Intercalation Mechanism in MXene Nanosheets, *ACS*

Nano, 2016, **10**, 3334–3341.

32 M. Okubo, A. Sugahara, S. Kajiyama and A. Yamada, MXene as a Charge Storage Host, *Acc. Chem. Res.*, 2018, **51**, 591–599.

33 L. Simonelli, C. Marini, W. Olszewski, M. Ávila Pérez, N. Ramanan, G. Guilera, V. Cuartero and K. Klementiev, CLAESS: The hard X-ray absorption beamline of the ALBA CELLS synchrotron, *Cogent Phys.*, 2016, **3**, 1231987.

34 B. Ravel and M. Newville, ATHENA, ARTEMIS, HEPHAESTUS: Data analysis for X-ray absorption spectroscopy using IFEFFIT, *J. Synchrotron Radiat.*, 2005, **12**, 537–541.

35 J. J. Rehr, R. C. Albers and S. I. Zabinsky, High-order multiple-scattering calculations of x-ray-absorption fine structure, *Phys. Rev. Lett.*, 1992, **69**, 3397–3400.

36 I. R. Shein and A. L. Ivanovskii, Graphene-like titanium carbides and nitrides Ti n+1C n, Ti n+1N n (n = 1, 2, and 3) from de-intercalated MAX phases: First-principles probing of their structural, electronic properties and relative stability, *Comput. Mater. Sci.*, 2012, **65**, 104–114.

37 E. A. Stern, Number of relevant independent points in x-ray-absorption fine-structure spectra, *Phys. Rev. B*, 1993, **48**, 9825–9827.

38 J. G. Chen, NEXAFS investigations of transition metal oxides, nitrides, carbides, sulfides and other interstitial compounds, *Surf. Sci. Rep.*, 1997, **30**, 1–152.

39 M. Magnuson, J. P. Palmquist, M. Mattesini, S. Li, R. Ahuja, O. Eriksson, J. Emmerlich, O. Wilhelmsson, P. Eklund, H. Högberg, L. Hultman and U. Jansson, Electronic structure investigation of Ti3AlC2, Ti3SiC2, and Ti3GeC2 by soft x-ray emission spectroscopy, *Phys. Rev. B - Condens. Matter Mater. Phys.*, 2005, **72**, 1–9.

40 M. Magnuson, O. Wilhelmsson, J. P. Palmquist, U. Jansson, M. Mattesini, S. Li, R. Ahuja and O. Eriksson, Electronic structure and chemical bonding in Ti2 AlC investigated by soft x-ray emission spectroscopy, *Phys. Rev. B - Condens. Matter Mater. Phys.*, 2006, **74**, 1–8.

41 C. A. Triana, C. M. Araujo, R. Ahuja, G. A. Niklasson and T. Edvinsson, Electronic transitions induced by short-range structural order in amorphous TiO2, *Phys. Rev. B*, 2016, **94**, 1–9.

42 M. Magnuson and L. Å. Näslund, Local chemical bonding and structural properties in Ti3AlC2MAX phase and Ti3C2Tx MXene probed by Ti1sX-ray absorption spectroscopy, *Phys. Rev. Res.*, 2020, **2**, 1–10.

43 F. Farges and G. E. Brown, Ti-edge XANES studies of Ti coordination and disorder in oxide

compounds: Comparison between theory and experiment, *Phys. Rev. B - Condens. Matter Mater. Phys.*, 1997, **56**, 1809–1819.

44 M. R. Lukatskaya, S. M. Bak, X. Yu, X. Q. Yang, M. W. Barsoum and Y. Gogotsi, Probing the Mechanism of High Capacitance in 2D Titanium Carbide Using in Situ X-Ray Absorption Spectroscopy, *Adv. Energy Mater.*, 2015, **5**, 2–5.

45 T. C. Rossi, D. Grolimund, M. Nachtegaal, O. Cannelli, G. F. Mancini, C. Bacellar, D. Kinschel, J. R. Rouxel, N. Ohannessian, D. Pergolesi, T. Lippert and M. Chergui, X-ray absorption linear dichroism at the Ti K edge of anatase TiO2 single crystals, *Phys. Rev. B*, 2019, **10**, 245207.

46 A. Lipatov, M. Alhabeb, M. R. Lukatskaya, A. Boson, Y. Gogotsi and A. Sinitskii, Effect of Synthesis on Quality, Electronic Properties and Environmental Stability of Individual Monolayer Ti3C2 MXene Flakes, *Adv. Electron. Mater.*, 2016, **2**, 1600255.

47 C. J. Zhang, S. Pinilla, N. McEvoy, C. P. Cullen, B. Anasori, E. Long, S. H. Park, A. Seral-Ascaso, A. Shmeliov, D. Krishnan, C. Morant, X. Liu, G. S. Duesberg, Y. Gogotsi and V. Nicolosi, Oxidation Stability of Colloidal Two-Dimensional Titanium Carbides (MXenes), *Chem. Mater.*, 2017, **29**, 4848–4856.

48 S. Huang and V. N. Mochalin, Hydrolysis of 2D Transition-Metal Carbides (MXenes) in Colloidal Solutions, *Inorg. Chem.*, 2019, **58**, 1958–1966.

49 Z. Li, L. Yu, C. Milligan, T. Ma, L. Zhou, Y. Cui, Z. Qi, N. Libretto, B. Xu, J. Luo, E. Shi, Z. Wu, H. Xin, W. N. Delgass, J. T. Miller and Y. Wu, Two-dimensional transition metal carbides as supports for tuning the chemistry of catalytic nanoparticles, *Nat. Commun.*, 2018, **9**, 1–8.

50 X. H. Wang and Y. C. Zhou, Layered Machinable and Electrically Conductive Ti2AlC and Ti3AlC2 Ceramics: a Review, *J. Mater. Sci. Technol.*, 2010, **26**, 385–416.

51 C. Shi, M. Beidaghi, M. Naguib, O. Mashtalir, Y. Gogotsi and S. J. L. Billinge, Structure of nanocrystalline Ti3C2 MXene using atomic pair distribution function, *Phys. Rev. Lett.*, 2014, **112**, 125501.

52 T. Yamamoto, Assignment of pre-edge peaks in K-edge x-ray absorption spectra of 3d transition metal compounds: electric dipole or quadrupole?, *X-Ray Spectrom.*, 2008, **37**, 572–584.

53 A. Gutierrez, N. A. Benedek and A. Manthiram, Crystal-chemical guide for understanding redox energy variations of M 2+/3+ couples in polyanion cathodes for lithium-ion batteries,

Chem. Mater., 2013, **25**, 4010–4016.

54 A. M. Abakumov, S. S. Fedotov, E. V. Antipov and J. M. Tarascon, Solid state chemistry for developing better metal-ion batteries, *Nat. Commun.*, 2020, **11**, 4976.

55 X. Wang, S. M. Bak, M. Han, C. E. Shuck, C. McHugh, K. Li, J. Li, J. Tang and Y. Gogotsi, Surface Redox Pseudocapacitance of Partially Oxidized Titanium Carbide MXene in Water-in-Salt Electrolyte, *ACS Energy Lett.*, 2022, **7**, 30–35.

56 D. C. Prins, R.; Koningsberger, Ed., *X-Ray Absorption: Principles, Applications, Techniques of EXAFS, SEXAFS, XANES*, Wiley, New York, 1988.

57 E. Sevillano, H. Meuth and J. J. Rehr, Extended x-ray absorption fine structure Debye-Waller factors. I. Monatomic crystals, *Phys. Rev. B*, 1979, **20**, 4908–4911.

58 J. J. Rehr and R. C. Albers, Theoretical approaches to x-ray absorption fine structure, *Rev. Mod. Phys.*, 2000, **72**, 621–654.

59 S. E. Ali, W. Olszewski, A. Sorrentino, C. Marini, A. Kazzazi, N. Laszczynski, A. Birrozzi, A. Mullaliu, S. Passerini, D. Tonti and L. Simonelli, Local Interactions Governing the Performances of Lithium- And Manganese-Rich Cathodes, *J. Phys. Chem. Lett.*, 2021, **12**, 1195–1201.

60 J. Lee, A. Urban, X. Li, D. Su, G. Hautier and G. Ceder, Unlocking the potential of cation-disordered oxides for rechargeable lithium batteries, *Science (80-.).*, 2014, **343**, 519–522.

61 J. Lee, D. H. Seo, M. Balasubramanian, N. Twu, X. Li and G. Ceder, A new class of high capacity cation-disordered oxides for rechargeable lithium batteries: Li-Ni-Ti-Mo oxides, *Energy Environ. Sci.*, 2015, **8**, 3255–3265.

62 R. Perriot, B. P. Uberuaga, R. J. Zamora, D. Perez and A. F. Voter, Evidence for percolation diffusion of cations and reordering in disordered pyrochlore from accelerated molecular dynamics, *Nat. Commun.*, 2017, **8**, 1–8.

63 R. J. Clément, Z. Lun and G. Ceder, Cation-disordered rocksalt transition metal oxides and oxyfluorides for high energy lithium-ion cathodes, *Energy Environ. Sci.*, 2020, **13**, 345–373.

64 Y. Yu, P. Karayaylali, D. Sokaras, L. Giordano, R. Kou, C. J. Sun, F. Maglia, R. Jung, F. S. Gittleson and Y. Shao-Horn, Towards controlling the reversibility of anionic redox in transition metal oxides for high-energy Li-ion positive electrodes, *Energy Environ. Sci.*, 2021, **14**, 2322–2334.

65 V. Kamysbayev, A. S. Filatov, H. Hu, X. Rui, F. Lagunas, D. Wang, R. F. Klie and D. V.

Talapin, Covalent surface modifications and superconductivity of two-dimensional metal carbide MXenes, *Science (80-.).*, 2020, **369**, 979–983.

66 Y. Li, H. Shao, Z. Lin, J. Lu, L. Liu, B. Duployer, P. O. Å. Persson, P. Eklund, L. Hultman, M. Li, K. Chen, X. H. Zha, S. Du, P. Rozier, Z. Chai, E. Raymundo-Piñero, P. L. Taberna, P. Simon and Q. Huang, A general Lewis acidic etching route for preparing MXenes with enhanced electrochemical performance in non-aqueous electrolyte, *Nat. Mater.*, 2020, **19**, 894–899.